Application and Evaluation of the Global Weather Research and Forecasting (GWRF) Model

Joshua Hemperly, Xin-Yu Wen, Nicholas Meskhidze, and Yang Zhang*
Department of Marine, Earth, and Atmospheric Sciences,
North Carolina State University, Raleigh, NC, USA, 27695

1. INTRODUCTION

The Weather Research and Forecasting (WRF) Model is a newly developed numerical weather prediction system for both atmospheric research and operational forecasting. The Global WRF (GWRF) in the latest WRF Version 3.0 (WRFV3) released in April, 2008, is an extension of previous versions of mesoscale WRF. Mesoscale WRF was modified by Mark Richardson's group at the California Institute of Technology (CalTech) beginning in 2004 for application to the Earth's global atmosphere through three key modifications: modification of projection from conformal to non-conformal grid, addition of a filter for polar boundary conditions, and adaptation of planetary constants and timing parameters for Earth (Richardson et al., 2005). GWRF, initially designed to study the atmospheres and climate systems of other planets such as Titan and Mars, enables modeling of global climate of the Earth system and the coupling between weather systems on global and regional scales (Richardson et al., 2007).

One of the main advantages of using GWRF is to provide initial and boundary conditions for the mesoscale version of WRF that ensures self-consistency of model physics. The main objective of this study is to evaluate the capability of GWRF for an accurate representation of the global atmosphere by comparing model output with observational data. Such an evaluation is a critical step toward the extension of GWRF to include emissions and chemical mechanisms needed to simulate the global transport of air pollutants, the impact of emissions on global air quality and radiative forcing, as well as the forecasting of future climate and air quality.

In this work, GWRF simulations are conducted for the year 2001. Model evaluation is conducted to assess the accuracy of GWRF in reproducing observations and to examine the model sensitivity to horizontal grid resolutions and cloud microphysics schemes.

**Corresponding author:* Yang Zhang, Department of Marine, Earth, and Atmospheric Sciences, Campus Box 8208, NCSU, Raleigh, NC, 27695; phone number: (919) 515-9688; fax number: (919) 515-7802; email: yang_zhang@ncsu.edu

2. MODELING APPROACH

2.1 Model Simulation Design

The baseline GWRF simulation is conducted at a horizontal grid resolution of 1° latitude × 1° longitude. Major parameterizations include WRF Single Moment 3-class (WSM3) microphysics, Kain-Fritsch cumulus parameterization, Goddard shortwave radiation, Community Atmosphere Model (CAM 3.0) long-wave radiation, the Yonsei University (YSU) planetary boundary layer (PBL) scheme, and the NOAH land-surface model (LSM). Model simulations at a coarse horizontal grid resolution of 4° latitude × 5° longitude are compared with that at 1° × 1° to study the relationship between model accuracy and grid resolution. GWRF has a vertical resolution of 27 layers from the surface to 50 mb. An additional simulation at 1° × 1° but with a complex ice microphysics scheme (i.e., the WRF Single Moment 6-class (WSM6)) is also conducted to examine the model sensitivity to cloud microphysics schemes, particularly to the ice treatments. The major difference between the WSM3 and WSM6 schemes is the number of hydrometeor classes. WSM3 treats three categories of hydrometeors (i.e., vapor, cloud water/ice, and rain/snow), whereas WSM6 treats six (i.e., vapor, rain, snow, cloud ice, graupel, and cloud water).

2.2 Model Initialization

GWRF is initialized using the WRF Preprocessing System version 3.0 (WPS3) which was released in April, 2008. The data used as input into WPS3 is from the National Center for Environmental Prediction (NCEP) Final Global Data Assimilation System (FNL) available from the WRF user's website. The NCEP FNL is the same dataset that is used to initialize a well known and commonly-used global atmospheric model, the Global Forecasting System (GFS), and has a horizontal grid resolution of one degree and a

temporal resolution of six hours. This dataset was chosen to initialize GWRF because of its temporal resolution and its common use in the WRF community. WPS is also used to create weekly sea surface temperature (SST) files for nudging of ocean temperatures, as recommended for simulations longer than one week (Skamarock et al., 2008). The model is constrained to 2001 by using the appropriate weekly FNL datasets in WPS for GWRF.

3. MODEL EVALUATION

3.1 Evaluation Protocol

Model evaluation focuses on major boundary layer meteorological variables including a combination of non-convective and convective weekly accumulated precipitation (RAINC+RAINNC), 2-meter temperature (T2) and water vapor mixing ratio (Q2), and 10-meter wind velocities and their zonal (U10) and meridional (V10) components, as well as radiation variables such as downward shortwave flux (SWDOWN) and downward long-wave radiation at the surface (GLW). The overall performance of GWRF is evaluated in terms of spatial distribution, seasonal and temporal variations, and statistics such as mean bias (MB), normalized mean bias (NMB), and correlation coefficient (Corr) over the global domain, the Northern and Southern Hemispheres, and the six populated continents. Model performance is also evaluated for the six general circulation cells: the Northern and Southern Polar, Ferrel, and Hadley Cells.

3.2 Datasets for Model Evaluation

The model reanalysis dataset used for GWRF evaluation is the NCEP/National Center for Atmospheric Research (NCAR) Reanalysis. To evaluate GWRF precipitation output, the Tropical Rainfall Measuring Mission (TRMM), the Climate Prediction Center Merged Analysis of Precipitation (CMAP), and the Global Precipitation Climatology Project (GPCP) datasets are used. To evaluate GWRF radiation output, the Baseline Surface Radiation Network (BSRN) and Global Energy Balance Archive (GEBA), as well as regional observational networks such as the surface radiation network (SURFRAD) and AmeriFlux networks are used. Finally, meteorological data from surface-based networks that cover the entire globe such as the National Climactic Data Center (NCDC) hourly global surface data are used, along with surface networks based over the United States such as the Clean Air Status and Trends Network (CASTNET) and the Speciated Trends Network (STN).

4. DISCUSSIONS

4.1 Annual Mean 2-m Temperature and Specific Humidity

Figure 1 shows the spatial distributions of mean biases of annual-mean T2 between GWRF results at 1°x 1° and 4°x 5° and NCEP/NCAR reanalysis. Figure 1(a) shows a maximum MB of 11.09 °C, and a minimum MB of -9.05 °C. In the 1°x 1° horizontal grid resolution simulation, large T2 biases occur over large mountain areas (e.g., the Andes Mountains in South America and the Tibetan Plateau in Asia) and Polar Regions. Small NMBs (not shown) occur in the Tropics (0.46% in the Northern Hadley Cell and 0.73% in the Southern Hadley Cell), particularly near the equator and larger negative NMB values occur over the Northern Polar Cell (-10.65%). Table 1 shows performance statistics for the six populated continents. NMBs for all six continents are less than 10%, with correlation coefficients above 0.93, indicating that GWRF has an acceptable performance for near surface temperatures over populated regions. Surface temperatures simulated by GWRF simulations at the finer grid resolution agree with guidelines set by the Intergovernmental Panel on Climate Change (IPCC), in which the majority of contemporary models exhibit an absolute error (simulated-observed) of less than 2°C outside of data-poor regions (i.e., the Poles) and regions of sharp elevation changes (Randall et al., 2007). GWRF globally averaged MB values fall within the range set by Randall et al. (2007), with values of -0.02 °C for the fine resolution case, and a slightly larger MB value of -0.07 °C for the coarse resolution case. The notable exception is Asia, over which warm bias is most likely due to the T2 error associated with the complex terrain of the Tibetan Plateau. Figure 1(b) shows, that a decrease in horizontal grid resolution from 1°x 1° (Figure1(a)) to 4°x 5° slightly worsens the biases over the large mountain areas (e.g., the Andes Mountains and the Tibetan Plateau) and Polar Regions (i.e., Greenland and Antarctica). Small NMBs (0.70% in the Northern Hadley Cell and 0.37% in the Southern Hadley Cell) occur in the Tropics. Figure 1(b) shows a maximum MB of 15.77 °C, and a minimum MB of -11.55 °C. An Examination of globally averaged GWRF Corr values (not shown) results in high Corr values for both fine (1.00) and

coarse (0.99) grid resolution cases. These GWRF Corr values are similar to the correlation coefficient for annual mean surface temperature between contemporary models and observations (0.98) reported by Randall et al. (2007).

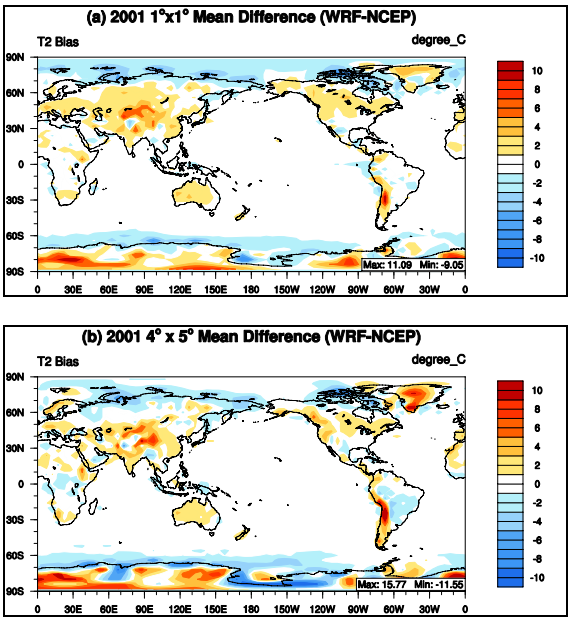

Figure 1. Spatial distributions of T2 mean biases between GWRF and NCEP/NCAR Reanalysis at (a) 1°x 1° and (b) 4°x 5°.

Table 1. T2 statistics over the six populated continents for the two grid resolutions. N.A. stands for North America and S.A. stands for South America.

Domain (1°x 1°)	MeanObs (°C)	MeanMod (°C)	Corr	NMB (%)
Europe	7.19	7.73	0.97	7.38
Africa	22.75	22.86	0.93	0.46
Asia	8.97	10.17	0.99	13.29
Australia	21.02	21.88	0.98	4.08
N.A.	10.90	11.39	0.99	4.54
S.A.	16.32	16.55	0.98	1.42
Domain (4°x 5°)	**MeanObs (°C)**	**MeanMod (°C)**	**Corr**	**NMB (%)**
Europe	7.19	7.4	0.94	2.82
Africa	22.75	22.89	0.87	0.61
Asia	8.97	9.62	0.99	7.2
Australia	21.02	21.79	0.98	3.68
N.A.	10.9	11.27	0.99	3.48
S.A.	16.32	16.51	0.94	1.18

In addition to near surface temperatures it is also important for GWRF to correctly reproduce observed zonal mean vertical profile of temperatures. The evaluation of the mean bias aloft has several implications including the performance of the overall global atmospheric temperature, and the potential impact of temperatures aloft on the vertical transport of gases and aerosols if these species were included in GWRF. Figure 2 shows that most zonal mean biases of temperature are within ±3 °C from the surface to 100 hPa (16 km), with a maximum MB of 6.8 °C and a minimum MB of about -13.7 °C for both fine and coarse grid resolution cases. Figure 2 shows that the highest positive and negative temperature biases are observed near the surface and above 200 hPa level, respectively. Such large, negative temperatures biases (particularly above the tropopause at high latitudes) are outside the ±2°C standard set by the IPCC (Randall et al., 2007).

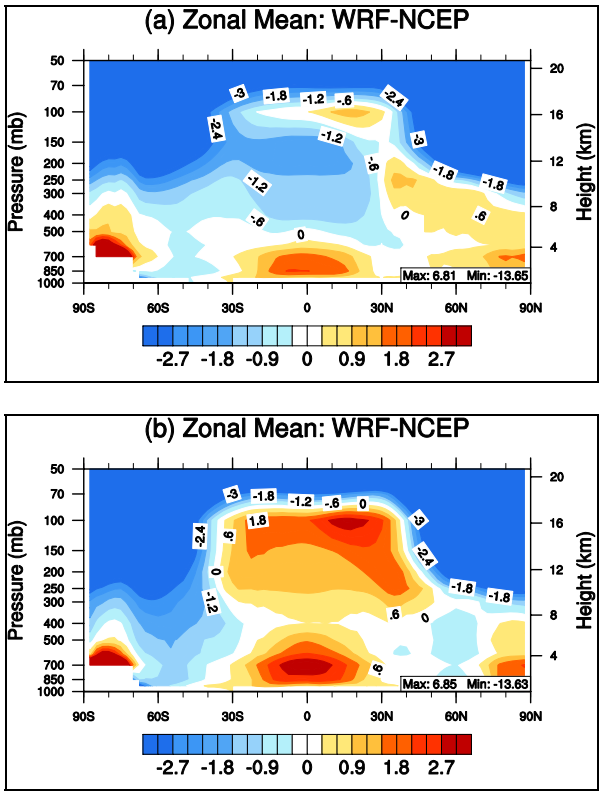

Figure 2. Zonal mean biases of temperatures between GWRF and NCEP/NCAR Reanalysis at (a) 1°x 1° and (b) 4°x 5°.

Water vapor mixing ratio at 2 meters above the surface (Q2) is an important boundary layer meteorological variable that strongly affect surface fluxes. In the 1°x 1° simulation, the largest biases occur over Tropical oceanic waters (30° N to 30° S) where GWRF slightly overestimates (~2 g kg^{-1}) Q2. The spatial distribution of Q2 also displays a slight underestimation (~2 g kg^{-1}) over the majority

of land surfaces. Due to the minimal amounts of water vapor in the Polar Regions, the largest NMBs of -8.87% and -10.31% occur in the Northern and Southern Polar Cells, respectively. The smallest NMBs of -0.38% and -0.56% occur in the Northern and Southern Hadley Cells, respectively. The Globally averaged NMB is -2.28%. For the fine grid resolution case, the majority of the six populated continents' NMBs are within ±10%, with correlation coefficients above 0.94. A decrease in horizontal grid resolution to 4°x 5° worsens the MB values for Q2 with a similar pattern of slight overestimation over equatorial oceans and a slight underestimation over major land surfaces. Overall, for the coarse grid resolution case, NMBs for the six populated continents are also negative within a range of ±10% and correlation coefficients higher than 0.91.

4.2 Shortwave and Longwave Radiation

The evaluation of the annual incoming shortwave radiation flux is important as an imbalance in the radiation budget in GWRF may result in inaccuracies in other meteorological fields. Figure 3 shows the apparent underestimation of incoming solar radiation in the high northern latitudes, and an overestimation over the Tropics and the Southern Ocean. In the 1°x 1° simulation, the largest NMBs (not shown) occur in the Tropics (15.54% and 16.91% in the Northern and Southern Hadley Cells, respectively). The Southern Hemispheric mean also exhibits a NMB of 11.66%. The Globally-averaged NMB is 7.77%. The majority of MB values are ±50 W m^{-2} annually, with a maximum MB of 115 W m^{-2} and a minimum MB of -89.4 W m^{-2}.

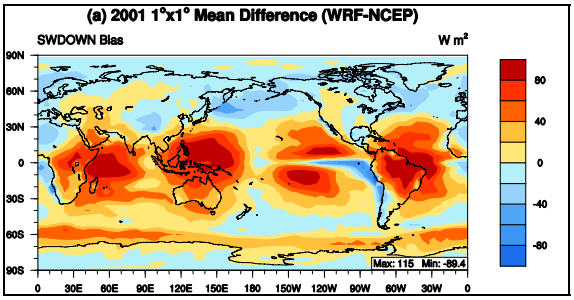

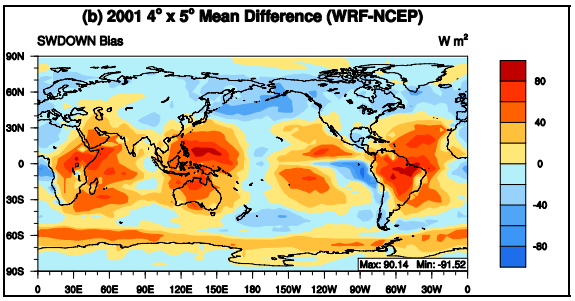

Figure 3. Spatial distributions of SWDOWN mean biases between GWRF and NCEP/NCAR Reanalysis at (a) 1°x 1° and (b) 4°x 5°.

Among the six populated continents, continents mainly in the Southern Hemisphere display the poorest statistical performance. The largest NMBs occur in South America (18.57%) and in Australia (18.50%), while other continents have NMBs within ±10%. The smallest correlation coefficients occur in Africa (0.49) and South America (0.78), while those for other continents are greater than 0.91.

Table 2. SWDOWN statistics over the six populated continents for the two grid resolutions. N.A. stand for North America and S.A. stands for South America.

Domain (1°x 1°)	MeanObs (W m^{-2})	MeanMod (W m^{-2})	Corr	NMB (%)
Europe	171.27	163.49	0.97	-4.54
Africa	267.64	287.87	0.49	7.56
Asia	215.06	225.34	0.92	4.78
Australia	240.79	285.33	0.91	18.50
N.A.	211.89	212.90	0.91	0.47
S.A.	208.86	247.65	0.78	18.57
Domain (4°x 5°)	**MeanObs (W m^{-2})**	**MeanMod (W m^{-2})**	**Corr**	**NMB (%)**
Europe	171.27	157.01	0.97	-8.32
Africa	267.64	282.22	0.55	5.45
Asia	215.06	221.81	0.94	3.14
Australia	240.79	280.15	0.94	16.35
N.A.	211.89	203.84	0.95	-3.8
S.A.	208.86	237.68	0.83	13.8

A decrease in horizontal grid resolution from 1°x 1° to 4°x 5° worsens MBs for the SWDOWN, but the two different resolutions display a consistent spatial pattern of an underestimation in the high northern latitudes, and an overestimation over the Tropics and the Southern Ocean. The largest NMBs occur over the Tropics (10.24% and 10.26% in the Northern and Southern Hadley Cells, respectively). The Globally-averaged NMB is 3.77% (not shown). As shown in Figure 3(b),

the maximum MB for SWDOWN is 90.1 Wm^{-2}, while the minimum MB is -91.5 W m^{-2}. Among the six populated continents, continents located mainly in the Southern Hemisphere have the largest NMBs (e.g., 13.80% in South America and 16.35% in Australia), while other continents have NMBs within ±10%. Southern Hemispheric continents also have the smallest correlation coefficients (0.55 for Africa and 0.83 for South America), while Corr values for the other four continents are greater than 0.94. Although the spatial distribution of MB for incoming solar radiation has many anomalies, there is a definite pattern of an overestimation in the Northern and Southern Hadley cells. This overestimation is most likely related to an insufficient amount of clouds simulated in the Tropics by GWRF.

To examine the energy budget and radiation balance simulated in GWRF, the downward long wave flux at the surface is explored. Accurate representation of downward long wave flux radiation in GWRF is crucial for a long term simulation of the atmosphere on a global domain. An overall underestimation of downward long wave radiation by GWRF (not shown) indicates that there is less radiation flux being reflected back to the surface at night, which may result in a net cooling effect. A spatial distribution of MBs in downward long-wave radiation at the surface indicates an overall underestimation of GLW throughout the globe, with slight overestimations over elevated terrains such as Antarctica, the Tibetan Plateau, and Greenland. In the 1°x 1° simulation, the largest NMBs occur in the Tropics (-8.25% and -8.42% in the Northern and Southern Hadley Cells, respectively). The Globally-averaged NMB of GLW is -6.35%. GLW MB values are negative for all of the domains, with a maximum MB of 58.4 W m^{-2} and a minimum MB of -68.73 W m^{-2}. Over the six populated continents, NMBs are within ±10%, with correlation coefficients above 0.91. A decrease in horizontal grid resolution from 1°x 1° to 4°x 5° worsens MBs for GLW. In the 4°x 5° case, the largest NMBs occur over the Tropics (-7.34% and -7.31% in the Northern and Southern Polar Cells, respectively). The Globally-averaged NMB is -5.03%. The maximum MB in GLW is 74.79 W m^{-2}, while the minimum MB is -67.24 W m^{-2}. Over the six populated continents NMBs for GLW are all within ±10%, with correlation coefficients above 0.87.

4.3 Precipitation

Precipitation fields in GWRF are a critical way to evaluate meteorological model performance for the baseline physics configuration, as well as sensitivity to horizontal grid resolution and microphysics option. Figure 4 shows mean biases for simulated precipitation rates in the summer of 2001 (June, July, August) against the GPCP data. GWRF replicates the spatial distribution of heavy rainfall rates associated with convection at the Inter-tropical Convergence Zone (ITCZ), as well as the slightly northward location of the ITCZ during summer, as compared to the rest of the year. It overpredicts rainfall rates off of the western coast of Central America and Southeast Asia. Similar to simulation at 1°x 1° (Figure 4(a)), GWRF at 4°x 5° (Figure 4(b)) replicates the spatial pattern of heavy rainfall rates near the equator but overpredicts their magnitudes. The positive bias in tropical simulated precipitation rates suggests that GWRF at both resolutions may over-predict the strength of the convection. The spatial distribution of precipitation in GWRF is consistent with standards set by the IPCC. On a global scale, GWRF shows lower precipitation rates at high latitudes and higher precipitation rates near the equator, while on a regional scale it demonstrates maximums at the major convergence zones and tropical rainforests. Despite consistent spatial distribution, GWRF displays substantial precipitation biases in the Tropics. Inability to accurately simulate isolated convection, land-sea breezes, monsoon patterns, or large scale oscillations (i.e., El Nino, shifting of the ITCZ) are some of the common reasons for overestimation of precipitation in the Tropics by the global models (Randall et al., 2007).

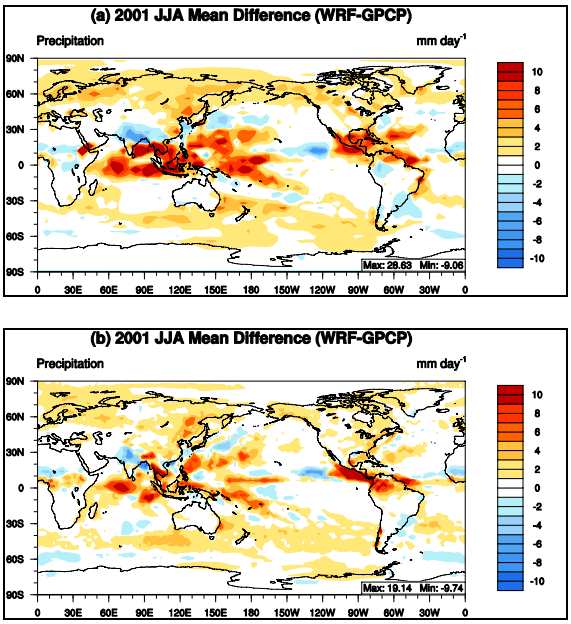

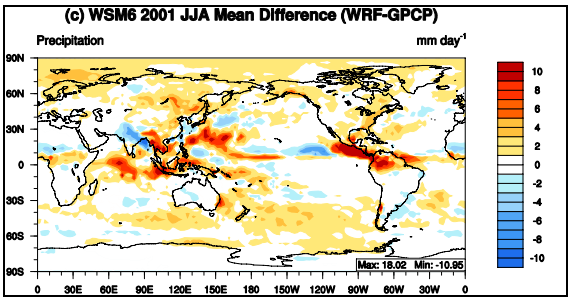

Figure 4. Spatial distributions of precipitation rate mean biases in summer 2001 between GWRF and GPCP at (a) 1°x 1° (b) 4°x 5° and (c) 1°x 1° using WSM6 microphysics.

Heavy precipitation in the Tropics as simulated by GWRF are similar for both the complex microphysics scheme (i.e., WSM6) and the simple microphysics scheme (i.e., WSM3). However, WSM6 alters the spatial distribution of precipitation rates compared to WSM3, especially over the western Pacific. The North Polar Region also displays an overestimation of precipitation for WSM6 simulation, which is absent in the WSM3 simulation.

5. SUMMARY

In this study, the GWRF predictions of 2-meter temperature and water vapor mixing ratio, downward shortwave and long-wave fluxes, and precipitation are evaluated against reanalysis data or satellite observations. The overall performance of GWRF for these variables at horizontal grid resolutions of 1°x 1° and 4°x 5° are examined. Accuracy in T2 model predictions is not greatly improved by using a finer horizontal grid resolution (1°x 1°); the Q2, SWDOWN, and GLW all exhibit an annual NMB within ±10% over the majority of the 6 populated continents. Despite the fact that GWRF was able to capture some of the global patterns of precipitation, rates for the summer of 2001 were over-predicted at both grid resolutions. Over-prediction was particularly pronounced near the Tropics. The complex microphysics scheme appears to suppress strong summer convection in the Tropics when compared with a simple microphysics scheme, indicating that the precipitation rates in the Tropics are sensitive to the ice treatment.

6. REFERENCES

Randall, D. A., R. A. Wood, S. Bony, R. Colman, T. Fichefet, J. Fyfe, V. Kattsov, A. Pitman, J. Shukla, J. Srinivasan, R. J. Stouffer, A. Sumi, and K.E. Taylor (2007), *Climate Change 2007: The Physical Science Basis. Contribution of Working Group I to the Fourth Assessment Report of the Intergovernmental Panel on Climate Change,* Climate Models and Their Evaluation, edited by Solomon, S., D. Qin, M. Manning, Z. Chen, M. Marquis, K.B. Averyt, M.Tignor and H.L. Miller, Cambridge University Press, Cambridge, United Kingdom and New York, NY, USA.

Richardson, M. I., A. D. Toigo, and C. E. Newman (2005), Non-conformal projection, global, and planetary versions of WRF, Presentation at the WRF/MM5 User's Workshop, Boulder Colorado.

Richardson, M. I., A. D. Toigo, and C. E. Newman (2007), PlanetWRF: A general purpose, local to global numerical model for planetary atmosphere and climate dynamics, *J. Geophy. Res., 112*, E09001.

Skamarock W. C., J. B. Klemp, J. Dudhia, D. O. Gill, D. M. Barker, M. G. Duda, X.-Y. Huang, W. Wang, and J. G. Powers (2008), A description of the Advanced Research WRF Version 3, NCAR Technical Note, 76, National Center for Atmospheric Research, Boulder, Colorado, USA.